BIOLOGICAL CRYSTALLOGRAPHY

ISSN 1399-0047

Structural insights into the binding of the human receptor for advanced glycation end products (RAGE) by S100B, as revealed by an S100B–RAGE-derived peptide complex

Jaime L. Jensen,[a]‡ Venkata S. K. Indurthi,[b]‡ David B. Neau,[c] Stefan W. Vetter[b]* and Christopher L. Colbert[a]*

[a]Department of Chemistry and Biochemistry, North Dakota State University, PO Box 6050, Fargo, ND 58108-6050, USA, [b]Department of Pharmaceutical Sciences, North Dakota State University, PO Box 6050, Fargo, ND 58108-6050, USA, and [c]NE-CAT, Bldg. 436E, Department of Chemistry and Chemical Biology, Cornell University, 9700 South Cass Avenue,, Argonne, IL 60439, USA. *Correspondence e-mail: stefan.vetter@ndsu.edu, christopher.colbert@ndsu.edu

Received 2 January 2015
Accepted 1 March 2015

Edited by R. McKenna, University of Florida, USA

‡ These authors contributed equally to this work.

Keywords: S100B; RAGE-derived peptide.

PDB reference: Ca^{2+}-S100B, complex with human RAGE-derived peptide, 4xyn

Supporting information: this article has supporting information at journals.iucr.org/d

S100B is a damage-associated molecular pattern protein that, when released into the extracellular milieu, triggers initiation of the inflammatory response through the receptor for advanced glycation end products (RAGE). Recognition of S100B is accomplished *via* the amino-terminal variable immunoglobulin domain (V-domain) of RAGE. To gain insights into this interaction, a complex between S100B and a 15-amino-acid peptide derived from residues 54–68 of the V-domain was crystallized. The X-ray crystal structure was solved to 2.55 Å resolution. There are two dimers of S100B and one peptide in the asymmetric unit. The binding interface of this peptide is compared with that found in the complex between S100B and the 12-amino-acid CapZ-derived peptide TRTK-12. This comparison reveals that although the peptides adopt completely different backbone structures, the residues buried at the interface interact with S100B in similar regions to form stable complexes. The binding affinities of S100B for the intact wild-type V-domain and a W61A V-domain mutant were determined to be 2.7 ± 0.5 and 1.3 ± 0.7 μ*M*, respectively, using fluorescence titration experiments. These observations lead to a model whereby conformational flexibility in the RAGE receptor allows the adoption of a binding conformation for interaction with the stable hydrophobic groove on the surface of S100B.

1. Background

The receptor for advanced glycation end products (RAGE) is a cell-surface pattern-recognition receptor of the immunoglobulin (Ig) superfamily (Neeper *et al.*, 1992) and a critical signaling molecule in disease progression through initiation of the inflammatory response (Clynes *et al.*, 2007). Overexpression of RAGE has been linked to multiple disease states, including cancer, Alzheimer's disease, cardiovascular disease and others. RAGE binds a variety of signaling molecules associated with cellular damage or stress, called damage-associated molecular pattern proteins (DAMPs), including the advanced glycation end products (AGEs), high mobility group box 1 (HMGB1), several components of the complement system (C3a, C1q and complement receptor 3) and the S100 proteins (Lotze *et al.*, 2007; Chavakis *et al.*, 2003; Leclerc *et al.*, 2009). Full-length RAGE consists of three immunoglobulin domains [the variable (V), constant 1 (C1) and constant 2 (C2) domains] in addition to a monotopic transmembrane helix and an unstructured cytoplasmic tail (Schmidt *et al.*, 1992). All extracellular domains (V, C1 and C2) are involved in recognizing diverse ligands, but the vast majority of ligands bind to

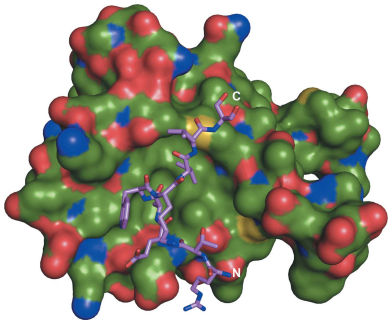

RAGE *via* the V-domain. It has been suggested that structural flexibility in the RAGE ectodomain accounts for its ability to bind variable DAMPs (Xie *et al.*, 2008; Sessa *et al.*, 2014).

One such DAMP, S100B, a member of the S100 protein family, is a calcium-binding, calmodulin-like regulator of numerous protein targets (Moore, 1965). Known S100B binding partners include other calcium-binding proteins (S100A1, annexin II and neurocalcin-δ), membrane-associated proteins (AHNAK, MARCKS and neuromodulin), various transcription factors (p53 and hdm2) and enzymes such as aldolase and protein kinase C (Donato, 2003; Heizmann, 2002). Each S100B monomer binds Ca^{2+} *via* two hinge-connected EF-hand motifs: a carboxy-terminal canonical EF-hand motif (Amburgey *et al.*, 1995) and an amino-terminal EF-hand motif distinct among S100 proteins (Fritz & Heizmann, 2004). Calcium binding exposes a large hydrophobic groove adjacent to helix 3 of S100B, which can accommodate interacting proteins or peptides. Although S100B has diverse intracellular functions, tissue damage results in release of the protein into the extracellular space, where it may encounter RAGE and initiate inflammatory signaling pathways in a cell-specific manner (Sparvero *et al.*, 2009; Meghnani *et al.*, 2014).

Recognition of its various ligands results in differential signal transduction by RAGE (Leclerc *et al.*, 2009; Zong *et al.*, 2010; Rai *et al.*, 2012; Xie *et al.*, 2013). Design of therapeutics to inhibit the RAGE–S100B interaction is complicated by a lack of structural information. Here, we report the 2.55 Å resolution crystal structure of S100B bound to a 15-amino-acid synthetic peptide that corresponds to residues 54–68 of RAGE. This structure reveals a new orientation for peptide binding on the surface of S100B that we compare with the S100B–TRTK-12 peptide interaction. This demonstrates that the hydrophobic groove on the surface of S100B is important for adapting the conformation of multiple binding partners to form stable interfaces. We provide binding data that support the moderate binding affinity of S100B to our peptide *via* primarily hydrophobic interactions and that verify the importance of the peptide residues in the S100B–RAGE interaction in the context of the RAGE V-domain. Finally, we discuss a potential binding model that implicates RAGE conformational flexibility for the multiple pattern-recognition capabilities of this receptor with different S100 proteins.

2. Materials and methods

2.1. Expression and purification of S100B and the RAGE V-domain

Recombinant dimeric human S100B was expressed and purified as described by Smith *et al.* (1996) and Ostendorp *et al.* (2005). The S100B dimer was isolated by size-exclusion chromatography and concentrated by centrifugation to 50 mg ml^{-1} in 25 m*M* Tris–HCl pH 7.8, 150 m*M* NaCl, 4 m*M* $CaCl_2$ using an Amicon Ultra-15 centrifugal filter unit with a nominal molecular-weight limit of 3000 Da (EMD Millipore).

The V-domain of RAGE (residues 23–132) was cloned into the pET-15b expression vector using the NcoI and XhoI restriction sites. Site-specific mutation of tryptophan to alanine (W61A) was achieved using the QuikChange site-directed mutagenesis kit (Stratagene). The plasmid region encoding the RAGE V-domain gene was sequenced to confirm mutagenesis and sequence integrity.

The V-domain protein was expressed in soluble form in the Shuffle T7 Express (New England Biolabs) *Escherichia coli* strain and was purified in two steps from the clarified cell lysate. An initial metal-chelate affinity chromatography step using HisTrap HP (GE Healthcare) columns was followed by a cation-exchange chromatography step using a HiTrap SP FF column (GE Healthcare). The purity of the protein was assayed by SDS–PAGE, which showed a protein single band at the expected molecular weight.

2.2. W61 peptide synthesis

The 15-amino-acid synthetic peptide corresponding to residues 54–68 of RAGE, hereafter referred to as W61, was synthesized using standard solid-phase peptide synthesis with Fmoc protection and HBTU/HOBt activation chemistry. To measure the binding affinities between W61 and S100B, a dansyl (Dns) fluorophore was coupled to the N-terminus of the peptide *via* a γ-aminobutyric acid (γAbu) spacer (Dns-W61). A mutant peptide (W61A) in which Trp61 was replaced by an alanine residue was synthesized in the same manner. The peptide used in the crystallization experiment did not contain the Dns-γAbu residues at its N-terminus. W61 peptides were released from the resin, the side chains were deprotected with 95% trifluoroacetic acid, 2.5% triisopropylsilane and 2.5% water and the peptides were purified by preparative HPLC to a single peak on an analytical HPLC column. MALDI-TOF mass spectrometry confirmed the expected molecular weight of the W61 peptides. The final sequences of the peptides used in titration experiments were Dns-γAbu-NTGRTEAWKVLSPQG-NH_2 (Dns-W61) and Dns-γAbu-NTGRTEAAKVLSPQG-NH_2 (Dns-W61A). The peptide used in crystallization had the sequence NH_2-NTGRTEAWKVLSPQG-NH_2.

2.3. Fluorescence titration of S100B and the RAGE V-domain peptide Dns-W61

Fluorescence titrations were performed by titrating S100B into 600 µl Dns-W61 and Dns-W61A peptides at a concentration of 2 µ*M* in 20 m*M* HEPES pH 7.4, 2 m*M* $CaCl_2$ and either 20 m*M* (low ionic strength) or 150 m*M* (high ionic strength) NaCl. Multiple dilutions of S100B (stock concentrations ranging from 227 to 2558 µ*M*) were used to limit the maximal total volume increase to <5%. Fluorescence emission spectra between 410 and 600 nm were recorded using an excitation wavelength of 340 nm. The change in fluorescence intensity at 510 nm was used to calculate the binding affinity between S100B and Dns-W61. The titrations were performed five times independently. The titration data were fitted using a modified quadratic equation model assuming 1:1 stoichiometry (Anderson *et al.*, 1988; Leclerc & Vetter, 1998).

2.4. Fluorescence titration of fluorescein-labeled S100B and the RAGE V-domain

S100B was labelled with fluorescein isothiocyanate (FITC) and the binding affinity between S100B and the wild type and the W61A mutant of the RAGE V-domain was determined by measuring the change in fluorescence polarization as a result of S100B–RAGE complex formation. The V-domain (at concentrations ranging from 2 to 230 µ*M*) was titrated into a solution of fluorescein-labeled S100B (1 µ*M*) in 30 m*M* Tris pH 7.1, 300 m*M* NaCl, 2 m*M* $CaCl_2$. Titrations were repeated at least three times and the best fit for the titration curves was obtained using a 1:1 RAGE:S100B stoichiometry model as described in §2.3.

2.5. Crystallization of the S100B–W61 complex

For co-crystallization of S100B and W61, 2 m*M* S100B was combined with 2 m*M* W61 peptide and stored on ice for ∼30 min prior to crystallization-tray setup. Crystallization trials were performed *via* the sitting-drop vapor-diffusion method by mixing 0.75 µl drops of S100B–W61 peptide with 0.75 µl reservoir solution consisting of 0.1 *M* sodium cacodylate pH 6.8, 25%(*w*/*v*) PEG 3350, 9 m*M* $CaCl_2$ and incubating at 20°C against 500 µl reservoir solution. Crystals were observed within one week, and were harvested and flash-cooled in liquid nitrogen using reservoir solution plus 20%(*v*/*v*) glycerol as a cryoprotectant prior to diffraction experiments.

2.6. Data collection and structure refinement

Diffraction data were collected under cryogenic conditions (∼100 K). The high-resolution diffraction data used for refinement were collected at a wavelength of 0.9792 Å on NE-CAT beamline 24-ID-C of the Advanced Photon Source (APS), Argonne, Illinois, USA. A data set from a single orthorhombic crystal was processed using *autoPROC* (Vonrhein *et al.*, 2011) with the pipeline components *MOSFLM* (Leslie, 1992) for autoindexing, *XDS* (Kabsch, 2010) and *SCALA* (Evans, 1997) for processing and *POINTLESS* (Evans, 2006) for space-group determination (see Table 1). The crystal belonged to space group $P2_12_12$, with unit-cell parameters a = 68.8, b = 86.7, c = 66.5 Å, and diffracted to 2.55 Å resolution. The crystal parameters differed from those previously reported for native (Ostendorp *et al.*, 2007) and peptide-bound S100B (Charpentier *et al.*, 2010).

The structure of S100B was determined by molecular replacement in *BALBES* (Long *et al.*, 2008), an automated MR pipeline in the *CCP*4 suite (Winn *et al.*, 2011), using a single monomer of multimeric Ca^{2+}-loaded human S100B (PDB entry 2h61; Ostendorp *et al.*, 2007) as a search model. The W61 peptide was manually built into the electron density in *Coot* (Emsley & Cowtan, 2004) by placing a polyalanine chain and mutating residues with strong $2F_o - F_c$ electron density. Initially, Arg57, Trp61 and Lys62 were modeled into the moderate electron density. The remaining residues were placed based on the W61 peptide sequence. Water O atoms were positioned using *PHENIX*, with subsequent visual verification. Refinement was carried out in *PHENIX* (Adams *et al.*, 2010). R_{work} converged to 20.3% and R_{free} to 25.4%. The final model includes four S100B molecules, eight coordinated Ca^{2+} ions, 35 water molecules and one copy of the W61 peptide per asymmetric unit (Table 1). The model was validated using *MolProbity* (Chen *et al.*, 2010) and no Ramachandran outliers were present (Table 1).

All figures were created using *PyMOL* v.1.5.0.4 (Schrödinger). Analyses of surface areas, protein interfaces, assemblies and interactions were determined using the *PISA* server (Krissinel & Henrick, 2007). R.m.s.d. comparisons were carried out in *PyMOL*. Atomic models and structure factors have been deposited in the Protein Data Bank as PDB entry 4xyn.

Table 1
X-ray diffraction data-reduction and refinement statistics.

Values in parentheses are for the highest resolution shell.

Data collection	
Beamline	24-ID-C, APS
Wavelength (Å)	0.9792
Space group	$P2_12_12$
Unit-cell parameters (Å, °)	a = 68.8, b = 86.7, c = 66.5, $\alpha = \beta = \gamma = 90$
Molecules in asymmetric unit	5
Resolution range (Å)	53.9–2.55
Total observations	35655
Unique observations	12930 (1304)
Multiplicity	2.8
Completeness (%)	95.7 (98.8)
R_{merge} (%)†	6.4 (46.8)
Average $I/\sigma(I)$	12.9 (2.2)
Data-processing program	*autoPROC*
Refinement	
Refinement program	*PHENIX*
Resolution range (Å)	53.9–2.55 (2.64–2.55)
R_{work} (%)	20.3
R_{free} (%)	25.4
R.m.s.d. stereochemistry	
Bond lengths (Å)	0.015
Bond angles (°)	1.50
Solvent content (%)	49.7
No. of atoms	
S100B	5703
W61 peptide	154
Waters	35
Ca^{2+}	8
Average B (Å^2)	
S100B	62.2
W61 peptide	66.6
Waters	50.4
Ca^{2+}	57.3
Ramachandran plot (%)	
Preferred	98
Allowed	2
Outliers	0
PDB code	4xyn

† $R_{merge} = \sum_{hkl}\sum_i |I_i(hkl) - \langle I(hkl)\rangle| / \sum_{hkl}\sum_i I_i(hkl)$.

3. Results

3.1. Structure of S100B in complex with the RAGE-derived W61 peptide

Crystals containing S100B in complex with the RAGE-derived W61 peptide belonged to the orthorhombic space

group $P2_12_12$, with unit-cell parameters a = 68.8, b = 86.7, c = 66.5 Å, and diffracted to 2.55 Å resolution (Table 1). Phasing was achieved using a single monomer of S100B (PDB entry 2h61) as the input model for molecular replacement, and four monomers were placed in the asymmetric unit as two homodimers: chains *A* and *B* and chains *C* and *D* (Fig. 1*a*). A single continuous region of unassigned electron density spanning the hydrophobic binding groove of chain *A* was found in both the $2F_o - F_c$ and the $F_o - F_c$ maps calculated from the initial molecular-replacement phases. This electron density was interpreted as the W61 peptide (chain *P*) and was confirmed by calculating a simulated-annealing composite OMIT map in *PHENIX* (Fig. 1*b*). Eight residues of the 15-amino-acid peptide were defined and modelled (Fig. 2). Despite an expected binding stoichiometry of 1:1 prior to crystallization, corresponding electron density was not found in equivalent locations for the other three S100B monomers (chains *B*, *C* and *D*) in the asymmetric unit. The reason for the absence of peptide density in monomers *B*, *C* and *D* is likely to be owing to steric interference between the noncrystallographically related monomers. In the case of the interface of chain *B* and chain *C*, positioning the peptide in equivalent positions as found in chain *A* results in a direct overlap of the peptide at the Leu64 position as well as clashes between the peptide Lys62 and S100B Glu87 side chains. An equivalent peptide position in chain *D* would result in a clash with Phe88 in a symmetry-related chain *A*. Further, there are slight variations on the surface of chain *D* that might contribute to a weakening of peptide binding.

The final refined model had an R_{work} of 20.3% and an R_{free} of 25.4%. The final model-refinement statistics are reported in Table 1. The S100B monomers were 95.7–98.9% complete, with missing residues corresponding to residues 91–92 in chain *A*, 92 in chain *B*, 92 in chain *C* and 89–92 in chain *D*. As expected, the S100B monomers exhibit an all-α fold with each monomer containing two EF-hand Ca^{2+}-binding motifs.

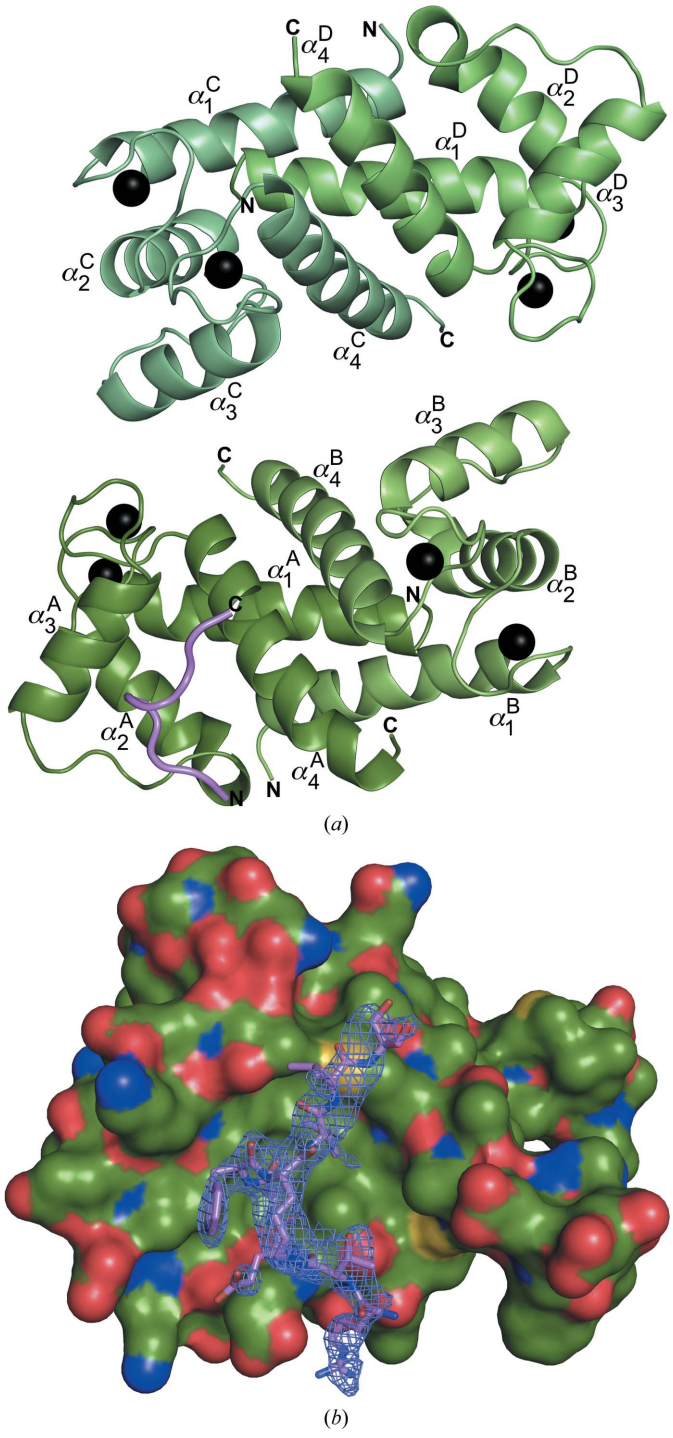

Figure 1
The asymmetric unit contents of the S100B–W61 crystal. (*a*) Two S100B homodimers and one W61 peptide are visible in the asymmetric unit. Monomers of S100B are shown in shades of green, the W61 peptide is shown in violet and Ca^{2+} ions are shown as black spheres. (*b*) Final refined $2F_o - F_c$ electron density (blue mesh) contoured at 1σ above the mean of the composite OMIT map shows the W61 peptide on the surface of S100B chain *A* in the same orientation as in (*a*).

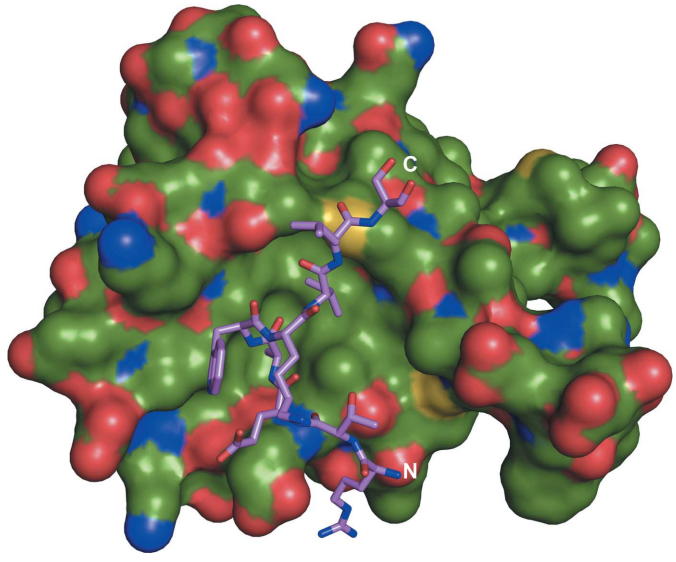

Figure 2
The S100B–W61 peptide complex. The surface of S100B is shown coloured according to atom type: carbon, green; oxygen, red; nitrogen, blue; sulfur, yellow. The W61 peptide is shown in stick representation and is coloured according to atom type: carbon, violet; oxygen, red; nitrogen, blue.

Overall, the structure of S100B is uniform within the crystal. Superposition of the four monomers (chains *A*, *B*, *C* and *D*) within the asymmetric unit yielded an overall root-mean-square deviation (r.m.s.d.) of 0.351–0.468 Å for 1076–1173 atoms from 88–91 residues. Minor variations were found in two regions. The C-termini of the monomers, which have already been shown to be quite flexible (Ostendorp *et al.*, 2007), exhibited variations as a result of the differing lengths of interpretable electron density. The second region is the hinge region (residues 43–54) between the EF-hands that connects helix 2 to helix 3. Side-chain density in the hinge region was occasionally limited to the C^{β} position. In these cases, the side chains were modelled in the most probable conformer that did not result in steric clashes, and the occupancies of atoms without electron density were set to 0.00 to prevent spurious negative peaks in the $F_o - F_c$ difference maps. Superposition of our S100B chain *A* on the monomer used as the search model during molecular replacement (PDB entry 2h61) gave an r.m.s.d. of 0.352 Å for all atoms, similar to the r.m.s.d. for the internal structure comparison.

3.2. Interaction of the RAGE-derived W61 peptide with S100B

The W61 peptide binds in the hydrophobic groove on the surface of S100B that has previously been shown to be the site of ligand binding (Charpentier *et al.*, 2010; McKnight *et al.*, 2012; Cavalier *et al.*, 2014). The peptide adopts an extended coil structure except for a three-residue 3_{10}-helical turn found in the middle of the peptide that positions Ala60, Trp61 and Val63 for packing against S100B to form the bulk of the complex interface (Fig. 2). The intervening residue between Trp61 and Val63, Lys62, is positioned away from interacting with S100B. The N-terminal and C-terminal ends of the peptide are well positioned to extend beyond the end of the hydrophobic groove (Fig. 2).

The interface between S100B and W61 was analysed using the *PISA* server (http://www.ebi.ac.uk/pdbe/pisa/). The complex buries a total of 485.6 Å^2, or 36.4% of the total surface area of the peptide. The association of W61 with S100B appears to be reliant on primarily hydrophobic interactions, as only two hydrogen bonds stabilize the interaction. Additionally, no salt bridges, disulfide bonds, covalent bonds or water molecules forming bridging hydrogen bonds were identified in the *PISA* analysis.

Binding of the W61 peptide to S100B did not induce a significant conformational change in S100B. As previously noted, the three monomers without peptide superimpose well with chain *A*. The superposition is comparable to the r.m.s.d.s between apo S100B and S100B in complex with a peptide derived from CapZ, TRTK-12 (an overall r.m.s.d. of 0.38 Å; Charpentier *et al.*, 2010). However, both of these nonhomologous peptides, W61 (NTG**RTEAWKVLS**PQG, where the

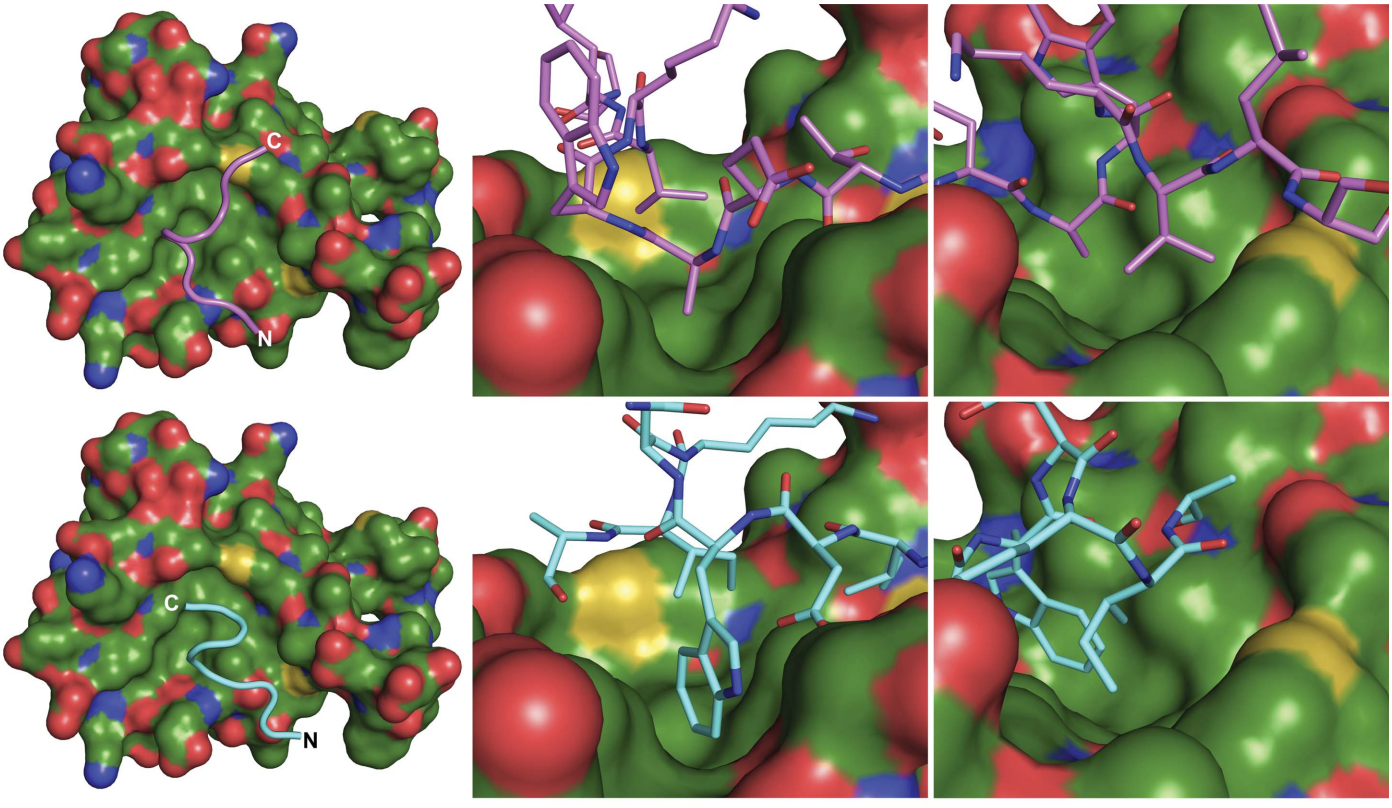

Figure 3
Comparison of the S100B–W61 (top) and S100B–TRTK-12 (bottom) crystal structures. (*a*) Cartoon representation of the peptide backbone (W61, violet; TRTK-12, cyan) on the surface of the hydrophobic groove of S100B. (*b*) Ala60 in the W61 peptide is positioned in the same pocket as the indole ring of Trp7 in TRTK-12. (*c*) Val63 of the W61 peptide is positioned in a groove formed by the surface of S100B residues Leu44, Phe76, Met79 and Val80 on the surface of S100B, similar to Ile10 in the TRTK-12 complex.

Table 2
Comparison of the buried surface area per S100B residue at the interface with the W61 and TRTK-12 peptides.

The total buried surface area for W61 was 913.6 Å^2 and that for TRTK-12 was 1084.3 Å^2. The value given is the percentage of the residue that is buried.

S100B residue	W61	TRTK-12 (PDB entry 3iqq)
Ile36	1.34	2.77
Ser41	17.55	11.35
His42	32.71	32.24
Phe43	23.13	42.94
Leu44	54.09	62.95
Glu45	81.39†	61.48
Glu46	0.29	2.09
Val52	36.43	21.08
Val56	35.33	29.80
Thr59	45.59	27.83
Leu60	1.01	0.00
Phe76	10.94	11.63
Met79	61.70	42.10
Val80	6.85	11.23
Ala83	16.71†	53.22
Cys84	0.00	13.90
Glu86	0.00†	21.48
Phe87	0.00	26.36

† Residue side chains not defined by electron density and modelled according to best-fit rotamers.

amino acids placed in the electron density of the X-ray structures are indicated in bold) and TRTK-12 (TR**TKIDWNKIL**S), bind in the hydrophobic groove on the surface of S100B, which has a significant amount of surface area contributed by the hinge region. Superposition of S100B–W61 chain *A* with the monomer of the S100B–TRTK-12 complex gave an r.m.s.d. of 0.477 Å. This is the result of greater conformational variations in the hinge region in the peptide-bound S100B complexes compared with the apo S100B structure. The minor flexibility in the hinge region combined with peptide flexibility allows the formation of different interaction interfaces for the two peptides (Fig. 3).

In the W61 peptide, Ala60 and Trp61 pack against hinge residues 45–54 of S100B. The hinge also plays a role in TRTK-12 binding. However, the presence of the Asp6 side chain in the TRTK-12 peptide, which hydrogen-bonds to the amide N atom of S100B Glu45, pushes the peptide backbone away from the hinge wall, allowing Trp7 to rotate into the depression occupied by peptide residue Ala60 in the W61 complex (Fig. 3*b*). Fundamentally, the difference in the involvement of the tryptophan in binding to S100B is that in the S100B–TRTK-12 structure Trp7 is 79.4% buried (141.2 Å^2) at the surface formed by helix 2 and the hinge region, while in the S100B–W61 structure Trp61 is only 34.7% buried (65.9 Å^2) and packs entirely against the hinge-loop region, allowing Ala60 to be positioned in the same location as the indole ring of Trp7 in TRTK-12 (Fig. 3*b*).

Another region of S100B variability between the two peptide complexes involves interactions at the amino-termini of the peptides. The orientation of the aromatic ring of S100B Phe43 in the S100B–W61 complex is shifted 0.3 Å and rotated by approximately 50° relative to the conformer found in S100B–TRTK-12. The conformer found in the TRTK-12 structure might be the result of the TRTK-12 peptide extending by an additional residue at its N-terminal end compared with the W61 peptide. While the W61 peptide has an additional three residues N-terminal to Arg57, the first ordered residue in the W61 peptide, there is no electron density to position them.

The final packing interaction of note involves the residues C-terminal to the tryptophan in both peptides. In the W61 complex, Val63 packs nicely into a hydrophobic pocket formed by Leu44 of the S100B hinge region and Phe76, Met79 and Val80 on helix 4 (Fig. 3*c*). The equivalent position is occupied by Ile10 in TRTK-12, which is held in place by the C-terminal residue, Leu11, looping back to hydrogen-bond the amide of Leu11 to the carboxylate of Trp7, similar to a β-turn. This tight bend in the TRTK-12 peptide prevents the C-terminal end of this peptide from further extension.

Despite the variability in the overall peptide-backbone conformation, the W61 and TRTK-12 peptides place the side chains of the different residues in similar locations in the hydrophobic groove on the surface of S100B. The difference between the buried surface area calculated for the S100B–W61 complex and that for the S100B–TRTK-12 complex is only 95.6 Å^2. This is primarily the result of two additional residues, Thr3 and Ile5, which provide additional interactions with residues on helix 4 in the TRTK-12 complex. Specific differences in the overall interactions of each peptide are summarized in Table 2.

3.3. Thermodynamics of the S100B–W61 peptide interaction

Fluorescence spectroscopy was used to quantify and to compare the binding of S100B to W61 at two salt concentrations. Titration of Dns-W61 into a solution of S100B under low ionic strength (20 m*M* NaCl) and high ionic strength (150 m*M* NaCl) conditions resulted in the determination of moderate binding affinities of 3 ± 1 and 14 ± 1 µ*M*, respectively. The best fit of the binding curve was obtained using a 1:1 stoichiometry of binding. A subsequent set of experiments assessed the role of Trp61 in binding by creating a Trp61-to-Ala mutant (Dns-W61A peptide) and performing similar titration experiments. Binding of the W61A peptide to S100B had a K_d of 4 ± 1 µ*M* under low ionic strength conditions and a K_d of 25 ± 2 µ*M* in the presence of 150 m*M* NaCl. These binding data indicate that the role of Trp61 in the interaction is likely to be limited to the part of the residue up to its C$^\beta$ atom, with only a minor contribution from the indole ring. As expected, binding of S100B to each peptide was Ca^{2+}-dependent and no binding was observed when titrations were performed in calcium-free buffers containing 2 m*M* EDTA.

To assess whether the affinity for the W61 peptide was relevant in the context of RAGE, we quantified and compared the binding of S100B to the wild-type RAGE V-domain and a W61A V-domain mutant. The S100B–V-domain interaction was measured by titrating the V-domain into a solution containing fluorescein-labelled S100B protein and the change in fluorescence polarization was measured. A K_d of 2.7 ± 0.5 µ*M* (R = 0.9938) was measured for the wild-type RAGE

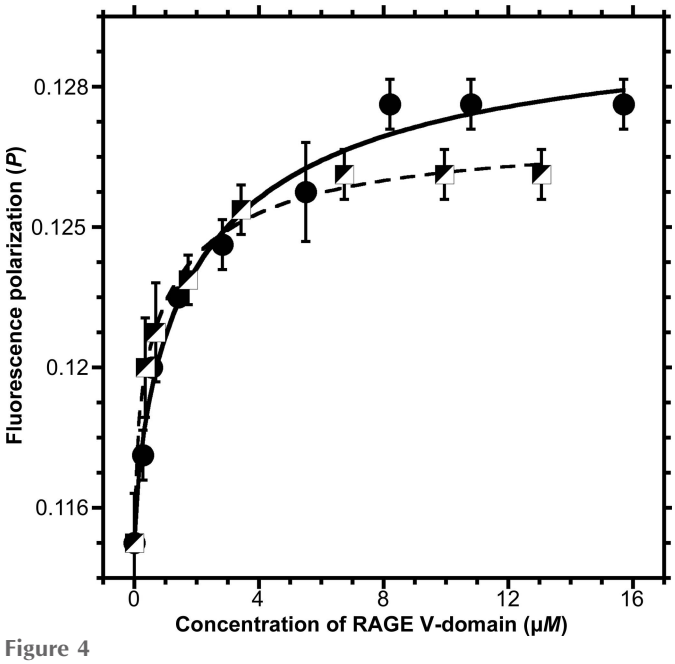

Figure 4
Fluorescence polarization titration of fluorescein-labeled S100B (1 μM) and the V-domain of RAGE. The titration of the wild-type V-domain is shown by black circles and that of the W61A mutant of the V-domain is shown by half-filled squares. The error bars indicate the standard deviation obtained from three independent experiments. The apparent K_d values obtain from the quadratic fits were 2.7 ± 0.5 μM (solid black line, $R = 0.9938$) and 1.3 ± 0.7 μM (dashed black line, $R = 0.9956$) for the wild-type V-domain and the W61A mutant, respectively (Anderson *et al.*, 1988; Leclerc & Vetter, 1998).

V-domain. When the same experiment was performed with the W61A V-domain mutant, the K_d improved to 1.3 ± 0.7 μM ($R = 0.9956$) (Fig. 4).

These thermodynamic data are in general agreement with the structural data. The dependence of the binding affinity on the ionic strength suggests a contribution from charge–charge or hydrogen-bonding interactions in the protein–peptide complex. The relatively minor change in RAGE–S100B binding affinity between the V-domain wild type and W61A mutant demonstrates that while this region is involved in S100B binding, the tryptophan residue is not critical for the interaction. This nicely reflects the observation that the indole ring of Trp61 is solvent-exposed in our crystal structure and not buried in the hydrophobic binding cavity of S100B.

4. Discussion

The crystal structure of the RAGE-derived W61 peptide in complex with S100B provides a potential structural model for the interaction between these two proteins. The structure of S100B is primarily unaltered by the presence of the W61 peptide. Binding between the W61 peptide and S100B may be driven by the stable hydrophobic groove found on the surface of S100B inducing the flexible peptide backbone to form optimal hydrophobic interactions. Examination of the S100B–TRTK-12 complex reveals that Trp7 is critical to the hydrophobic interaction in this groove. In the W61 peptide, mutation of the essentially equivalent Trp61 to alanine does not influence the specificity of S100B for the peptide because of the limited interaction of the indole ring with the surface wall of the hinge region in S100B. Instead, the W61 peptide backbone adopts a different conformation to that observed in the tryptophan interaction in the TRTK-12 structure. The W61 conformation positions the carbonyl of Val58 in an equivalent position to the Asp6 side chain in TRTK-12 and then places Ala60 and the main chain of Glu59 into the space occupied by the TRTK-12 tryptophan. Thus, this region of W61 forms a nearly equivalent, although unique, interface. The available NMR and X-ray structures of the RAGE V-domain indicate that the region encompassing the W61 peptide can adopt multiple conformations (Koch *et al.*, 2010; Xue *et al.*, 2011, 2014; Yatime & Andersen, 2013). Within this region, several structures have adopted a short, three-residue, antiparallel β-structure immediately after Trp61 (PDB entries 2l7u, 3cjj, 2mov and 4lp4; Koch *et al.*, 2010; Xue *et al.*, 2011, 2014; Yatime & Andersen, 2013). Other structures (PDB entry 2e5e; S. Matsumoto, T. Yoshida, I. Yasumatsu, K. Yamamoto, Y. Kobayashi & T. Ohkubo; Colbert, unpublished work) do not exhibit this secondary structure. However, in each structure Trp61 and Val63 are partially solvent-exposed, which positions them to potentially recognize the interaction surface on S100B. This provides an interesting model whereby the structural stability of S100B may force flexible regions, such as those found on the RAGE V-domain, to adopt conformations that favor the interaction in this hydrophobic groove.

This proposed model of an S100B-induced stable interface with a conformationally plastic peptide is further supported by our binding data for the W61A mutant. In the context of the flexible peptide, there was very little influence on binding between the native sequence and the W61A mutant. However, in the context of the RAGE V-domain, the affinity of the W61A mutant was enhanced by a factor of two relative to the wild-type V-domain. This is intuitively reasonable because the smaller alanine side chain would provide greater pliability in the V-domain backbone, allowing it to more easily adopt a conformation that would be complementary to the S100B hydrophobic groove. However, from the V-domain binding data, it cannot be ruled out that there are additional sites on the V-domain that might further stabilize or even provide alternate binding sequences to interact with RAGE. The model presented here would allow both of these possibilities. These alternative postulations will require further structural and biophysical investigations to fully understand how S100B and other S100 proteins can differentially modulate RAGE-mediated signalling.

Acknowledgements

This work was supported, in whole or in part, by National Institutes of Health Grants P20 RR015566 and P30 GM103332-01 and National Science Foundation Grant EPS-0814442 to CLC. VSKI was supported in part by an Infrastructure Improvement Program–Doctoral Dissertation Assistantship (IIP-DDA), North Dakota EPSCoR Grant: NSF#0814442. This work is based upon research conducted at the Advanced Photon Source on the Northeastern

Collaborative Access Team beamlines, which are supported by a grant from the National Institute of General Medical Sciences (P41 GM103403) from the National Institutes of Health. This research used resources of the Advanced Photon Source, a US Department of Energy (DOE) Office of Science User Facility operated for the DOE Office of Science by Argonne National Laboratory under Contract No. DE-AC02-06CH11357. JLJ thanks the experts at the CCP4/APS School in Macromolecular Crystallography as well as fellow student, Kip Guja in the laboratory of Dr Miguel Garcia-Diaz at SUNY Stony Brook, for their input in structure solution and refinement.

References

Adams, P. D. *et al.* (2010). *Acta Cryst.* D**66**, 213–221.
Amburgey, J. C., Abildgaard, F., Starich, M. R., Shah, S., Hilt, D. C. & Weber, D. J. (1995). *J. Biomol. NMR*, **6**, 171–179.
Anderson, K. S., Sikorski, J. A. & Johnson, K. A. (1988). *Biochemistry*, **27**, 1604–1610.
Cavalier, M. C., Pierce, A. D., Wilder, P. T., Alasady, M. J., Hartman, K. G., Neau, D. B., Foley, T. L., Jadhav, A., Maloney, D. J., Simeonov, A., Toth, E. A. & Weber, D. J. (2014). *Biochemistry*, **53**, 6628–6640.
Charpentier, T. H., Thompson, L. E., Liriano, M. A., Varney, K. M., Wilder, P. T., Pozharski, E., Toth, E. A. & Weber, D. J. (2010). *J. Mol. Biol.* **396**, 1227–1243.
Chavakis, T., Bierhaus, A., Al-Fakhri, N., Schneider, D., Witte, S., Linn, T., Nagashima, M., Morser, J., Arnold, B., Preissner, K. T. & Nawroth, P. P. (2003). *J. Exp. Med.* **198**, 1507–1515.
Chen, V. B., Arendall, W. B., Headd, J. J., Keedy, D. A., Immormino, R. M., Kapral, G. J., Murray, L. W., Richardson, J. S. & Richardson, D. C. (2010). *Acta Cryst.* D**66**, 12–21.
Clynes, R., Moser, B., Yan, S. F., Ramasamy, R., Herold, K. & Schmidt, A. M. (2007). *Curr. Mol. Med.* **7**, 743–751.
Donato, R. (2003). *Microsc. Res. Tech.* **60**, 540–551.
Emsley, P. & Cowtan, K. (2004). *Acta Cryst.* D**60**, 2126–2132.
Evans, P. R. (1997). *Jnt CCP4/ESF–EACBM Newsl. Protein Crystallogr.* **33**, 22–24.
Evans, P. (2006). *Acta Cryst.* D**62**, 72–82.
Fritz, G. & Heizmann, C. W. (2004). *Handbook of Metalloproteins*, edited by A. Messerschmidt, R. Huber, K. Weighardt & T. Poulos. Chichester: John Wiley & Sons. doi:10.1002/0470028637.met046.
Heizmann, C. W. (2002). *Methods Mol. Biol.* **172**, 69–80.
Kabsch, W. (2010). *Acta Cryst.* D**66**, 125–132.
Koch, M., Chitayat, S., Dattilo, B. M., Schiefner, A., Diez, J., Chazin, W. J. & Fritz, G. (2010). *Structure*, **18**, 1342–1352.
Krissinel, E. & Henrick, K. (2007). *J. Mol. Biol.* **372**, 774–797.
Leclerc, E., Fritz, G., Vetter, S. W. & Heizmann, C. W. (2009). *Biochim. Biophys. Acta*, **1793**, 993–1007.
Leclerc, E. & Vetter, S. W. (1998). *Eur. J. Biochem.* **258**, 567–571.
Leslie, A. G. W. (1992). *Jnt CCP4/ESF–EACBM Newsl. Protein Crystallogr.* **26**.
Long, F., Vagin, A. A., Young, P. & Murshudov, G. N. (2008). *Acta Cryst.* D**64**, 125–132.
Lotze, M. T., Zeh, H. J., Rubartelli, A., Sparvero, L. J., Amoscato, A. A., Washburn, N. R., DeVera, M. E., Liang, X., Tör, M. & Billiar, T. (2007). *Immunol. Rev.* **220**, 60–81.
McKnight, L. E., Raman, E. P., Bezawada, P., Kudrimoti, S., Wilder, P. T., Hartman, K. G., Godoy-Ruiz, R., Toth, E. A., Coop, A., MacKerell, A. D. Jr & Weber, D. J. (2012). *ACS Med. Chem. Lett.* **3**, 975–979.
Meghnani, V., Vetter, S. W. & Leclerc, E. (2014). *Biochim. Biophys. Acta*, **1842**, 1017–1027.
Moore, B. W. (1965). *Biochem. Biophys. Res. Commun.* **19**, 739–744.
Neeper, M., Schmidt, A. M., Brett, J., Yan, S. D., Wang, F., Pan, Y.-C. E., Elliston, K., Stern, D. & Shaw, A. (1992). *J. Biol. Chem.* **267**, 14998–15004.
Ostendorp, T., Heizmann, C. W., Kroneck, P. M. H. & Fritz, G. (2005). *Acta Cryst.* F**61**, 673–675.
Ostendorp, T., Leclerc, E., Galichet, A., Koch, M., Demling, N., Weigle, B., Heizmann, C. W., Kroneck, P. M. & Fritz, G. (2007). *EMBO J.* **26**, 3868–3878.
Rai, V., Maldonado, A. Y., Burz, D. S., Reverdatto, S., Yan, S. F., Schmidt, A. M. & Shekhtman, A. (2012). *J. Biol. Chem.* **287**, 5133–5144.
Schmidt, A. M., Vianna, M., Gerlach, M., Brett, J., Ryan, J., Kao, J., Esposito, C., Hegarty, H., Hurley, W., Clauss, M., Wang, F., Pan, Y.-C. E., Tsang, T. C. & Stern, D. (1992). *J. Biol. Chem.* **267**, 14987–14997.
Sessa, L., Gatti, E., Zeni, F., Antonelli, A., Catucci, A., Koch, M., Pompilio, G., Fritz, G., Raucci, A. & Bianchi, M. E. (2014). *PLoS One*, **9**, e86903.
Smith, S. P., Barber, K. R., Dunn, S. D. & Shaw, G. S. (1996). *Biochemistry*, **35**, 8805–8814.
Sparvero, L. J., Asafu-Adjei, D., Kang, R., Tang, D., Amin, N., Im, J., Rutledge, R., Lin, B., Amoscato, A. A., Zeh, H. J. & Lotze, M. T. (2009). *J. Transl. Med.* **7**, 17.
Vonrhein, C., Flensburg, C., Keller, P., Sharff, A., Smart, O., Paciorek, W., Womack, T. & Bricogne, G. (2011). *Acta Cryst.* D**67**, 293–302.
Winn, M. D. *et al.* (2011). *Acta Cryst.* D**67**, 235–242.
Xie, J., Méndez, J. D., Méndez-Valenzuela, V. & Aguilar-Hernández, M. M. (2013). *Cell. Signal.* **25**, 2185–2197.
Xie, J., Reverdatto, S., Frolov, A., Hoffmann, R., Burz, D. S. & Shekhtman, A. (2008). *J. Biol. Chem.* **283**, 27255–27269.
Xue, J., Rai, V., Singer, D., Chabierski, S., Xie, J., Reverdatto, S., Burz, D. S., Schmidt, A. M., Hoffmann, R. & Shekhtman, A. (2011). *Structure*, **19**, 722–732.
Xue, J., Ray, R., Singer, D., Böhme, D., Burz, D. S., Rai, V., Hoffmann, R. & Shekhtman, A. (2014). *Biochemistry*, **53**, 3327–3335.
Yatime, L. & Andersen, G. R. (2013). *FEBS J.* **280**, 6556–6568.
Zong, H., Madden, A., Ward, M., Mooney, M. H., Elliott, C. T. & Stitt, A. W. (2010). *J. Biol. Chem.* **285**, 23137–23146.